

Direct observation of interface and surface steps in epitaxial films by dark-field transmission electron microscopy

D. Loretto, F. M. Ross, C. A. Lucas, and G. C. L. Wong

Citation: [Applied Physics Letters](#) **65**, 1766 (1994); doi: 10.1063/1.112912

View online: <http://dx.doi.org/10.1063/1.112912>

View Table of Contents: <http://scitation.aip.org/content/aip/journal/apl/65/14?ver=pdfcov>

Published by the [AIP Publishing](#)

Articles you may be interested in

[Direct imaging of light elements by annular dark-field aberration-corrected scanning transmission electron microscopy](#)

Appl. Phys. Lett. **104**, 071908 (2014); 10.1063/1.4866185

[Three-dimensional shapes and distribution of FePd nanoparticles observed by electron tomography using high-angle annular dark-field scanning transmission electron microscopy](#)

J. Appl. Phys. **107**, 024304 (2010); 10.1063/1.3280026

[Atomic resolution composition analysis by scanning transmission electron microscopy high-angle annular dark-field imaging](#)

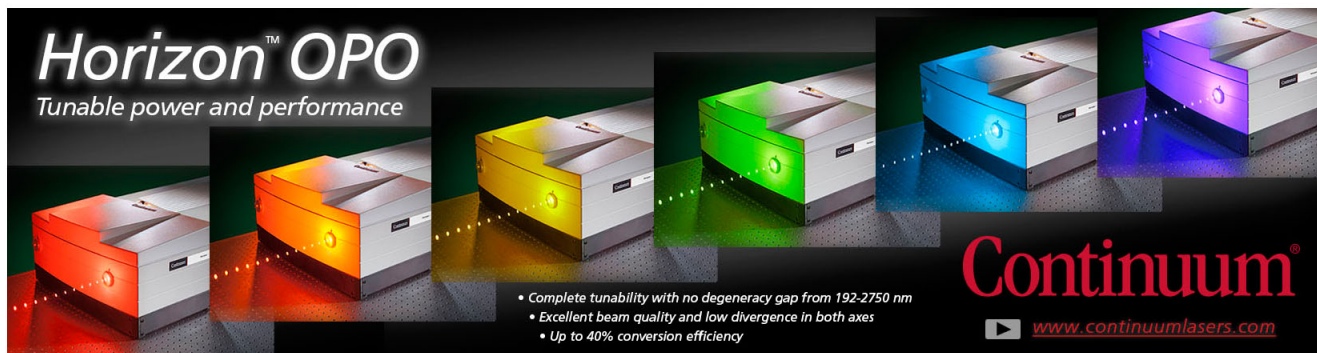
Appl. Phys. Lett. **83**, 662 (2003); 10.1063/1.1592314

[Direct observation of stacking fault tetrahedra in ZnSe/GaAs\(001\) pseudomorphic epilayers by weak beam dark-field transmission electron microscopy](#)

Appl. Phys. Lett. **71**, 1225 (1997); 10.1063/1.119858

[A Quantitative Method for the Study of Orientation Relationship between Subgrains by Dark-Field Transmission Electron Microscopy](#)

J. Appl. Phys. **37**, 2764 (1966); 10.1063/1.1782118

The advertisement features a row of five Continuum Horizon OPO laser units, each emitting a different color of light: red, orange, yellow, green, and blue. The text 'Horizon™ OPO' is prominently displayed in the top left, with the tagline 'Tunable power and performance' below it. In the bottom right, the Continuum logo is shown in red, with the website 'www.continuumlasers.com' and a play button icon. A list of features is provided in the bottom center:

- Complete tunability with no degeneracy gap from 192-2750 nm
- Excellent beam quality and low divergence in both axes
- Up to 40% conversion efficiency

Direct observation of interface and surface steps in epitaxial films by dark-field transmission electron microscopy

D. Loretto, F. M. Ross,^{a)} C. A. Lucas, and G. C. L. Wong^{b)}

Materials Sciences Division, Lawrence Berkeley Laboratory, Mail Stop 2-200, Berkeley, California 94720

(Received 14 February 1994; accepted for publication 22 July 1994)

We have used dark-field transmission electron microscopy to investigate <5 nm thick CaF₂ films grown on Si(111) by molecular-beam epitaxy. Images formed with CaF₂ [111] reflections exhibit contrast at 1/3[111] height steps at the CaF₂ surface and at the CaF₂/Si interface over large (>100 μm²), statistically significant areas. Direct evidence for step-flow growth in CaF₂ has been obtained.

© 1994 American Institute of Physics.

Atomic-height steps play a pivotal role in epitaxial growth and in other interface and surface mediated processes. Their distribution at the interfaces and surfaces of a thin film can have a direct impact on its electrical and optical properties. Transmission electron microscopy (TEM) is well suited to the observation of atomic-height steps at surfaces and interfaces, since it uses penetrating radiation (>100 keV electrons), has extremely high spatial resolution, and because the scattering is strong enough to allow an ordered monolayer to be detected. Atomic-height steps can be imaged either in high-resolution transmission electron microscopy (HRTEM) using cross-section specimens (where the electron beam is at grazing incidence to the interface) or by diffraction contrast performed on plan-view specimens (with the electron beam at high incident angle to the interface/surface). HRTEM samples an extremely small area of interface (<0.01 μm² for each cross-section specimen), and only high-symmetry beam directions lying in the plane of the interface can be accessed. Furthermore, HRTEM images are not easily interpretable, because of multiple scattering and the influence of parameters such as objective lens defocus and lens aberrations. The high electron energy (>200 keV) and dose also causes radiation damage in many materials. Diffraction-contrast images from plan-view specimens are better suited for the observation of atomic-height steps. Large (>100 μm²), statistically significant areas of surface and interface can be imaged in a single plan-view specimen and the incident electron beam is not constrained to high-symmetry directions. Image contrast is also simpler to interpret, since the scattering can often be treated kinematically and because parameters such as objective lens defocus and lens aberrations do not have a critical influence on contrast. In low magnification TEM the electron dose is several orders of magnitude less than that in HRTEM.

Atomic-height steps on the surfaces of plan-view TEM specimens have been seen in diffraction-contrast images from a number of materials, including Au,¹ MgO,^{2,3} and Si.^{4,5} These observations were performed using either conventional TEM instruments and nonreactive materials (Au and MgO)^{1,2,3} or ultrahigh-vacuum (UHV) TEM instruments, preparing clean surfaces *in situ*.^{4,5} In only a few cases

have atomic-height steps in thin films been studied using diffraction contrast. Atomic-height steps at the surface of Ag platelets on MoS₂ have been imaged by UHV TEM⁶ and interface steps have been observed in mixed-orientation (partially twinned)⁷ and in single-orientation, twinned⁸ CoSi₂/Si(111) using conventional TEM instruments.

Two other techniques have recently been employed to image atomic-height steps in thin films. Scanning probe microscopy has been used to image steps in NiSi₂/Si(111),⁹ and contrast from steps and interfacial defects has been seen in low-energy electron microscopy (LEEM) images of Ag islands on Si.¹⁰ Since very different electron energies are used in each technique, information obtained by LEEM and scanning probe microscopy is complementary to that obtained by plan-view TEM. TEM has the advantage that images from steps can be easily combined with diffraction-contrast analysis of other crystal defects. LEEM and scanning probe microscopy images are less easy to interpret but have the advantage that the substrate need not be prethinned.

In this letter we report, for the first time, the use of TEM to directly observe the distribution of atomic-height interface and surface steps in an epitaxial film over large, statistically significant areas. In this work we use CaF₂/Si(111) grown by molecular-beam epitaxy (MBE), though the method is more generally applicable. CaF₂ is a face-centered-cubic material with a lattice parameter only 0.6% larger than Si at room temperature. Single-orientation, pseudomorphic CaF₂ films as thin as 1.5 nm can be grown on Si(111).¹¹

Well-oriented (<1° miscut) Si(111) substrates were cleaned using the Shiraki method¹² and were loaded into a Riber MBE system. The Si wafers were outgassed at 600 °C before desorption of the oxide at 900 °C and CaF₂ was evaporated from a BN effusion cell at 1150 °C. Substrate temperatures were measured using a W/Re thermocouple in thermal contact with the back face of the sample, calibrated using an optical pyrometer and the Si(111)1×1–7×7 transition temperature as observed by *in situ* reflection high-energy electron diffraction. The pressure of the system was in the low 10⁻¹⁰ Torr range during growth. Samples were capped at room temperature with amorphous Si (*a*-Si) before removal from the vacuum system. Film thicknesses were either measured directly by x-ray crystal truncation rod scattering,¹¹ or were inferred from the relative intensity of “film” and “interface” components in Ca 2*p* x-ray photoelectron signals measured *in situ*.¹³ Plan-view TEM specimens were prepared

^{a)}Also at National Center for Electron Microscopy, Lawrence Berkeley Laboratory.

^{b)}Also at Department of Physics, University of California, Berkeley.

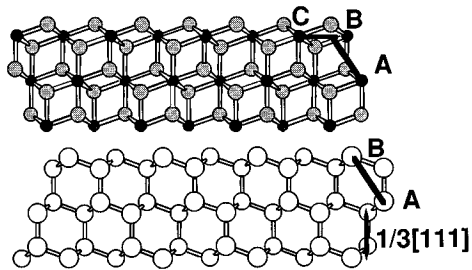


FIG. 1. A model of $\text{CaF}_2/\text{Si}(111)$ viewed along $[1\bar{1}0]$: Open circles represent Si atoms; circles shaded gray are F, and black circles are Ca. The bulk coordination of the Ca (eightfold) and Si and F (fourfold) is indicated by “sticks” connecting nearest neighbors. The twin orientation is visible as a 180° rotation about $[111]$.

by etching 0.1 mm thick Si discs in $\text{HF}:\text{HNO}_3$ diluted 1:7 and were examined in a JEOL 200 CX electron microscope equipped with a side entry, double-tilt goniometer specimen stage and a $5\ \mu\text{m}$ diameter objective aperture.

Figure 1 is a model of $\text{CaF}_2/\text{Si}(111)$ viewed along $[1\bar{1}0]$. The smallest step height in Si and CaF_2 is $1/3[111]$ (0.31 nm), corresponding to the addition or removal of either a Si bilayer or a CaF_2 triple layer (TL). (A CaF_2 TL is equivalent to a single F-Ca-F molecular layer.) Since CaF_2 grows in a twinned orientation, rotated 180° about $[111]$, the translation symmetry between CaF_2 and Si is broken.¹⁴ The vector AB, which connects equivalent Si sites below and above a $1/3[111]$ step, requires a further translation, BC, to connect equivalent sites in twinned CaF_2 . This broken-translational symmetry leads to the formation of a line defect with a displacement of $BC(1/6[11\bar{2}])$ wherever there is a $1/3[111]$ step on the Si surface. The wafers used in this study all have a small miscut ($<1^\circ$) from the exact $[111]$ direction, giving regularly spaced, parallel bilayer steps on the Si surface, which, in turn, result in regularly spaced, parallel line defects at the $\text{CaF}_2/\text{Si}(111)$ interface.¹⁵ Figure 2(a), which was taken using a strongly excited $\text{Si}[2\bar{2}0]$ reflection, shows an array of broken-translation-symmetry line defects at the interface between Si(111) and a 1.5 nm thick CaF_2 film. A few of the line defects visible in Fig. 2(a), for example the short defects running perpendicular to the broken-translation-symmetry defects, show contrast consistent with a Burgers vector along $\langle 110 \rangle$ (the analysis is not presented here). These are presumably misfit relieving dislocations, since the primary slip system in bulk CaF_2 is $1/2\langle 110 \rangle$ on $\{001\}$.¹⁶ The change in contrast on either side of two line defects in the lower right-hand corner of Fig. 2(a) is due to the buckling of the thinned TEM specimen¹⁷ in the presence of two $1/2\langle 110 \rangle$ type dislocations which, in this case, happen to lie along $1/3[111]$ interfacial steps. The broken-translation-symmetry, i.e., $1/6[11\bar{2}]$, and misfit-relieving, i.e., $1/2\langle 110 \rangle$, line defects are not the only defects in the film. Triangular regions lying within individual terraces and small strain centers are also visible.

Figure 2(b) shows the same region as Fig. 2(a), imaged in dark field with $\text{CaF}_2[11\bar{1}]$ close to the exact Bragg condition. Changes in thickness of 1 CaF_2 TL (0.31 nm) appear as a change in brightness of the image. Two sets of steps are visible. The parallel steps, which are correlated with the ar-

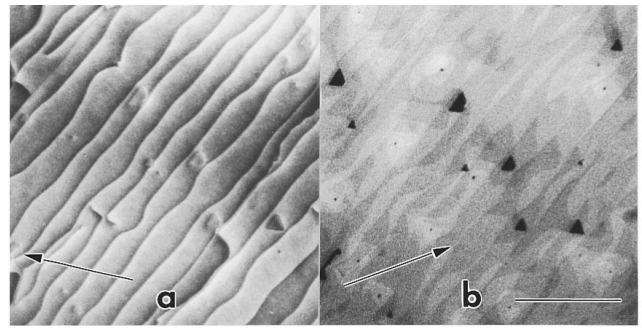


FIG. 2. Two-beam TEM images taken from the same region of an $\alpha\text{-Si}/\text{CaF}_2/\text{Si}(111)$ sample. The deposition time was 140 s and the substrate temperature was 770°C , giving a film thickness of ~ 5 CaF_2 TLs. The diffraction vectors are marked and the scale bar is $0.5\ \mu\text{m}$. (a) is a $\text{Si}[2\bar{2}0]$ dark-field image taken with the incident beam within a few degrees of $[111]$. (b) is the same region imaged with $\text{CaF}_2[11\bar{1}]$ with the incident beam direction close to $\text{Si}[12\bar{3}]$.

ray of $1/6[11\bar{2}]$ line defects seen in Fig. 2(a), are $1/3[111]$ steps at the $\text{CaF}_2/\text{Si}(111)$ interface. The more curved steps are at the $\text{CaF}_2(111)$ surface buried under amorphous Si. The contrast change across an interface step is the same as that across a surface step, as is apparent in regions where the two sets of steps intersect. The CaF_2 surface steps are therefore also $1/3[111]$ (1 TL) high. (The TL step height is expected because it is known that CaF_2 evaporates as F-Ca-F molecules.) The misfit-relieving dislocations do not change the thickness of the CaF_2 film and therefore show no contrast in Fig. 2(b). The triangular features seen in Fig. 2(a) appear dark in the $\text{CaF}_2[11\bar{1}]$ image in Fig. 2(b). It has previously been shown that growth at high temperatures proceeds via a reacted $\text{CaF}_2\text{-Si}$ surface layer upon which 3–4 TL thick CaF_2 islands nucleate, grow, and coalesce to form a continuous film.¹³ The 3–4 TL thick CaF_2 islands are bounded by Si(111) surface steps and are elongated along surface terraces. The triangular features visible in Figs. 2(a) and 2(b) are holes in the film where the islands have not completely coalesced. The gray level next to each hole in Fig. 2(b) corresponds to the same thickness of either 3 or 4 TLs. The smaller strain centers visible in Figs. 2(a) and 2(b) are presumably SiC particles, which commonly occur on Si surfaces cleaned using the Shiraki method. The SiC particles sometimes pin the Si $1/3[111]$ surface steps, giving cusps in the $\text{CaF}_2/\text{Si}(111)$ interface steps, which can be seen in the strain contrast image in Fig. 2(a) and the thickness contrast image in Fig. 2(b). The SiC particles also influence the morphology of the top surface, acting as secondary nucleation sites for CaF_2 growth, leading to surface steps circling each SiC particle. The presence of well defined surface steps is direct evidence for step-flow growth of CaF_2 at 700°C .

To understand the contrast in the $\text{CaF}_2[11\bar{1}]$ image shown in Fig. 2(b), it is useful to consider the reciprocal lattice for Si and twinned CaF_2 , drawn schematically in Fig. 3. The $\text{CaF}_2[11\bar{1}]$ reflection is coincident with the forbidden, weak Si $1/3[51\bar{1}]$ reflection. Images taken with the $\text{CaF}_2[11\bar{1}]$ reflection set close to the Bragg condition will therefore be dominated by scattering in the CaF_2 . Furthermore, if the CaF_2 film thickness is much less than the

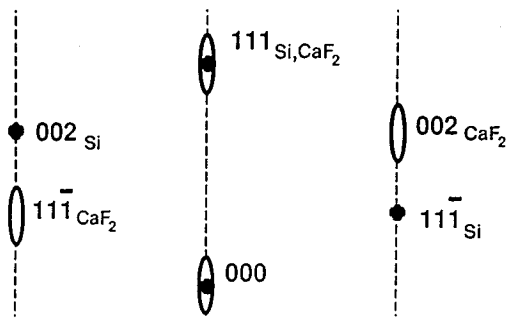


FIG. 3. A $\langle 112 \rangle$ section through the reciprocal lattices for twinned CaF_2 on $\text{Si}(111)$. Si reciprocal lattice points are black circles. CaF_2 reciprocal lattice maxima are ellipses. The dashed line lies along $[111]$.

$\text{CaF}_2[11\bar{1}]$ extinction length, as is the case in Fig. 2(b), multiple scattering can be neglected and image brightness will be proportional to film thickness. This second approximation is no longer valid for large deviations from the Bragg condition, which decrease the effective extinction length. The step contrast in Fig. 2(b) vanishes if the sample is tilted 4° away from the Bragg condition, leaving contrast from line defects, SiC particles, and holes in the film. The thickest CaF_2 films we have successfully imaged using $\text{CaF}_2[11\bar{1}]$ reflections are ~ 20 TLs thick. This limitation is due to increased diffuse scattering from the Si, since plan-view TEM samples, which are prepared by etching away the Si substrate, require thicker Si backing to prevent thicker, strained, CaF_2 films from relaxing. In Fig. 2(b) we use an extremely small, $5 \mu\text{m}$ diameter, objective aperture to exclude as much diffuse background as possible.

Figure 4 shows further examples of dark-field images taken using $\text{CaF}_2[11\bar{1}]$ reflections from $a\text{-Si}/\text{CaF}_2(111)$ grown under different conditions and on wafers of different miscut. The step separation and the density of SiC are markedly different in each case. The long-range influence of the SiC particles on CaF_2 surface steps is especially apparent in Fig. 4(a). The $\text{CaF}_2(111)$ surface step distribution visible in Fig. 4(b) is, in the absence of a high density of SiC particles, correlated with the step distribution on the $\text{Si}(111)$ surface as dictated by the miscut. The film is thick enough for the 3–4 TL high islands which form in the initial stages of $\text{CaF}_2/\text{Si}(111)$ growth to have almost completely coalesced. There is also evidence for faceting of the surface steps along $\langle 011 \rangle$.

In conclusion, we have shown how dark-field TEM can be used to determine the distribution of atomic-height steps at top and bottom interfaces of an epitaxial film over large areas ($>100 \mu\text{m}^2$). Direct evidence for step-flow growth of $\text{CaF}_2/\text{Si}(111)$ has been obtained from dark-field $\text{CaF}_2[11\bar{1}]$

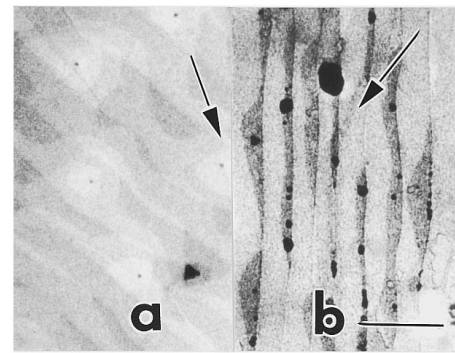


FIG. 4. Two-beam $\text{CaF}_2[11\bar{1}]$ images taken from samples grown at (a) 700°C with a deposition time of 72 s and (b) 770°C with a deposition time of 140 s. The incident beam direction is close to $\text{Si}[123]$ and the $0.5 \mu\text{m}$ scale bar applies to both figures. The $\text{CaF}_2[11\bar{1}]$ diffraction vectors are marked as arrows.

images. The method uses conventional TEM instruments and, in the cases where the film and substrate scattering are separable, can be applied to other materials systems. The observed contrast is also simple to interpret. We anticipate that the dark-field technique described here will be extremely powerful when applied, *in situ*, to thin-film growth.

D. L. would like to acknowledge helpful discussions with Steve Yalisove, T. T. Cheng, Mark Aindow, and Kevin Heim. This work was supported by the Director, Office of Basic Energy Sciences, Materials Sciences Division of the U.S. Department of Energy under Contract No. ACO3-76SF00098.

- ¹D. Cherns, *Philos. Mag.* **B30**, 549 (1974).
- ²G. Lempfuhr and Y. Uchida, *Ultramicroscopy* **4**, 275 (1979).
- ³G. Lempfuhr and C. E. Warble, *Ultramicroscopy* **19**, 135 (1986).
- ⁴J. M. Gibson and M. Y. Lanzerotti, *Nature* **340**, 128 (1989).
- ⁵F. M. Ross and J. M. Gibson, *Phys. Rev. Lett.* **68**, 1782 (1992).
- ⁶G. Lempfuhr and K. Takayanagi, *Ultramicroscopy* **6**, 195 (1981).
- ⁷A. C. Daykin and C. Kiely, *MRS Proc.* **263**, 243 (1992).
- ⁸R. T. Tung and J. P. Sullivan (private communication).
- ⁹J. A. Kubby and W. J. Greene, *Phys. Rev. Lett.* **68**, 329 (1992).
- ¹⁰R. M. Tromp, A. W. Dernier van der Gon, F. K. LeGoues, and M. C. Reuter, *Phys. Rev. Lett.* **71**, 3299 (1993).
- ¹¹C. A. Lucas and D. Loretto, *Appl. Phys. Lett.* **60**, 2071 (1992).
- ¹²A. Ishizaka and Y. Shiraki, *J. Electrochem. Soc.* **133**, 666 (1986).
- ¹³G. C. L. Wong, D. Loretto, E. Rotenberg, M. A. Olmstead, and C. A. Lucas, *Phys. Rev. B* **48**, 5716 (1993); C. A. Lucas, D. Loretto, and G. C. L. Wong, *Phys. Rev. B* (to be published).
- ¹⁴R. C. Pond, *CRC Crit. Rev. Solid State Mater. Sci.* **15**, 441 (1989).
- ¹⁵The relationship between Si surface topography and broken-translation-symmetry, $1/6[11\bar{2}]$, line defects has been studied extensively in the crystallographically equivalent systems $\text{CoSi}_2/\text{Si}(111)$ and $\text{NiSi}_2/\text{Si}(111)$. See, for example, R. T. Tung and F. Schrey, *Appl. Phys. Lett.* **54**, 852 (1989).
- ¹⁶R. N. Katz and R. L. Coble, *J. Appl. Phys.* **45**, 2376 (1974).
- ¹⁷R. Siems, P. Delavignette, and S. Amelinckx, *Phys. Status Solidi* **2**, 421 (1962).